A high-speed magnetic tweezer beyond 10,000 frames per second

Bob M. Lansdorp, Shawn J. Tabrizi, Andrew Dittmore, and Omar A. Saleh'

Citation: Rev. Sci. Instrum. **84**, 044301 (2013); doi: 10.1063/1.4802678
View online: http://dx.doi.org/10.1063/1.4802678
View Table of Contents: http://aip.scitation.org/toc/rsi/84/4
Published by the American Institute of Physics

A high-speed magnetic tweezer beyond 10,000 frames per second

Bob M. Lansdorp,[1] Shawn J. Tabrizi,[2] Andrew Dittmore,[1] and Omar A. Saleh[3,a)]
[1]*Materials Department, University of California Santa Barbara, Santa Barbara, California 93106, USA*
[2]*College of Creative Studies, University of California Santa Barbara, Santa Barbara, California 93106, USA*
[3]*Materials Department and Biomolecular Science and Engineering Program, University of California Santa Barbara, Santa Barbara, California 93106, USA*

(Received 9 March 2013; accepted 8 April 2013; published online 29 April 2013)

The magnetic tweezer is a single-molecule instrument that can apply a constant force to a biomolecule over a range of extensions, and is therefore an ideal tool to study biomolecules and their interactions. However, the video-based tracking inherent to most magnetic single-molecule instruments has traditionally limited the instrumental resolution to a few nanometers, above the length scale of single DNA base-pairs. Here we have introduced superluminescent diode illumination and high-speed camera detection to the magnetic tweezer, with graphics processing unit-accelerated particle tracking for high-speed analysis of video files. We have demonstrated the ability of the high-speed magnetic tweezer to resolve particle position to within 1 Å at 100 Hz, and to measure the extension of a 1566 bp DNA with 1 nm precision at 100 Hz in the presence of thermal noise. © *2013 AIP Publishing LLC*. [http://dx.doi.org/10.1063/1.4802678]

I. INTRODUCTION

Single-molecule manipulation (SMM) instruments such as the magnetic tweezer, optical tweezer, and atomic force microscope (AFM) measure individual bio-molecules and their interactions with salt, proteins, and other molecules.[1,2] The development of high-resolution SMM instruments, in particular optical tweezers with sub-nanometer resolution at a bandwidth of hundreds of Hertz, has catalyzed the discovery of many new bio-physical phenomena.[1,3–7] New instrumental techniques that allow for the measurement of many molecules in parallel with improved accuracy will continue to provide insights into the nature of biological machines at the nanoscale.[8,9]

Optical and magnetic tweezers can be contrasted in how they apply force to probe particles. Whereas an optical tweezer typically traps a probe particle in an energetic potential well, a magnetic tweezer applies a constant force to the probe particle. A constant force avoids complications arising from changes to the potential energy landscape that are generated by molecular motions against a changing load.[10] Furthermore, since the bead displacement signal-to-noise ratio is independent of trapping stiffness,[11] a constant force instrument can measure single molecule activity such as the step size of a motor protein without the added complication of a feedback-based passive force clamp.[10]

The optimal SMM instrument maximizes spatial resolution over a large measurement bandwidth, and is very stable.[12] Traditionally, the magnetic tweezer has been the lower-resolution companion to the optical tweezer, with video-rate tracking listed as the reason for limited bandwidth measurements.[2] Although attempts have been made to increase the spatial resolution of the magnetic tweezer using specially coated beads,[13] these attempts have thus far been incapable of the low thermal noise required of high-resolution tracking. Sensitivity to thermal noise beyond the Nyquist frequency is possible using strobed light sources;[14] however, for non-stationary processes such as motor protein stepping, light strobing cannot be used to artificially enhance the data acquisition rate. The recent introduction of high-speed cameras to particle tracking[15–17] has opened the door to a new field of video-based single-molecule manipulation that can obtain high spatial and temporal resolution. Here, we fulfilled the requirement for sufficient light at high frames rates with a superluminescent diode (SLD), replaced the conventional 60 Hz CCD with a high-speed CMOS (hs-CMOS) camera, and introduced a graphics processing unit (GPU)-based tracking algorithm for improved data throughput. We used our high-speed magnetic tweezer to demonstrate spatial resolution and bandwidth comparable to a high-resolution optical tweezer instrument.

II. MAGNETIC TWEEZER OPERATION

The magnetic tweezer measures the dynamics of single molecules by observing the three-dimensional position of magnetic probe particles. The probe particles are typically tethered to the surface of a glass coverslip, and are subjected to forces between 0.1 pN and 50 pN, depending on the applied magnetic field. Video-based images of probe particles are sent to a computer processor to convert images into three-dimensional positions.[8,18]

A. Illumination

The magnetic tweezer tracks particle position by imaging the interference pattern of a reference wave (typically a collimated LED) and scattered light from a probe particle. The ideal light source to create high quality interference patterns has a high power, a relatively short coherence length, and a single spatial mode. A high-power illumination source allows for high-speed tracking over a large field-of-view. A relatively short coherence length reduces image artifacts such

a)Electronic mail: saleh@engineering.ucsb.edu

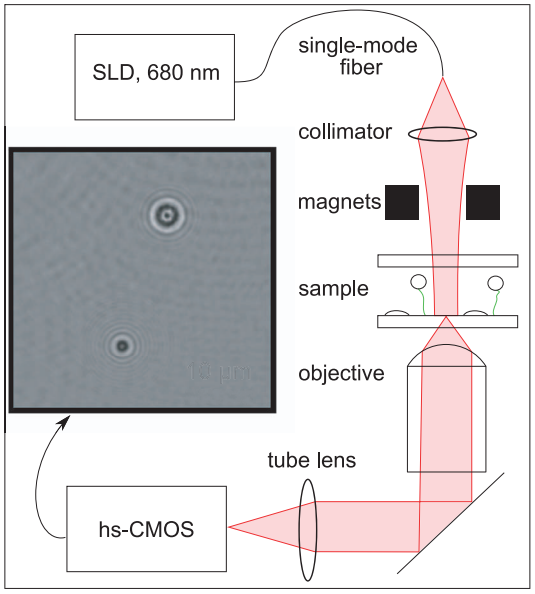

FIG. 1. A schematic of the high-speed magnetic tweezer with a fiber-coupled superluminescent diode (SLD) for illumination and a high-speed CMOS (hs-CMOS) camera for detection. The inset shows a 256 × 256 8-bit brightfield-normalized still-frame, taken from a video acquired at 35 087 fps. The still frame shows a partially molten 2.5 μm diameter reference bead and a 1.05 μm diameter streptavadin-coated magnetic bead, which is tethered to the surface via a DNA hairpin.

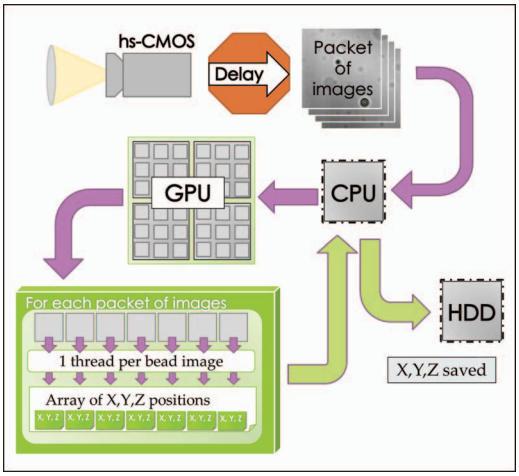

FIG. 2. Schematic illustration of data flow in our high-speed magnetic tweezer. Images from the hs-CMOS camera are transferred (with delay) via ethernet cable to the CPU. The CPU transfers the data to the GPU, where XYZ coordinates are generated.

as speckle and noise from stray reflections in the optical path, while retaining enough coherence to create sharp diffraction rings around each bead. A single spatial mode permits creation of a tight collimated beam, allowing the magnets to translate over a large distance without distorting the image on the sample plane. Furthermore, a single spatial mode allows the bead diffraction patterns to be imaged over a large focal range.

To meet the guidelines for an ideal light source, we have introduced a 2 mW SLD (QPhotonics) to our magnetic tweezer. The SLD has a spectral width of 7.9 nm at a central wavelength of 680 nm. We fiber-coupled the SLD through a 0.12 Numerical Aperture (NA) single-mode fiber, and collimated it using a 7.5 mm focal length fiber collimator (Thorlabs). Light from the SLD passed through custom-designed magnets,[19] was scattered by beads in our flowcell, and collected by a 100 × 1.4 NA Nikon objective into a Nikon TE2000-U inverted microscope, where it was routed to the high-speed camera (see Figure 1 for schematic). The SLD has a similar temporal coherence as an LED, but since the SLD is single-mode, we observed bead diffraction patterns to be sharper. Furthermore, we observed that the single-mode SLD permitted improved collimation, resulting in a narrow-waisted beam that minimized clipping of light on the magnets and permitted the magnets to be translated over a larger range.

B. High-speed video capture

To increase the temporal resolution of the magnetic tweezer, we have used a high-speed camera (Vision Research Phantom v7.3-16GB) in place of the previously used CCD (Jai CV-A10). The high-speed camera can capture up to 180 000 frames per second (fps) at a reduced field-of-view. With a typical 256 × 256 pixel field-of-view, the camera can capture 35 087 fps and store 6.9 s of video on the 16 GB of onboard memory. The subsequent transfer of video frames from onboard camera memory to the CPU happens via a Gigabit ethernet connection at approximately 25 MB/s, which corresponds to a transfer speed of 380 fps. A schematic of the data-flow in our high-speed magnetic tweezer is shown in Figure 2.

To reduce the effect of non-uniform background illumination, we transformed the raw image I_{raw} using bright-field normalization.[20] The bright-field image I_{BF} was taken by manually scanning the sample laterally, and taking the median image intensity at each pixel of approximately fifty frames. The dark field I_{DF} was taken by blocking the light source. The bright-field normalized pixel intensity for an 8-bit image is then

$$I_{normalized}(x, y) = 100\left(\frac{I_{raw}(x, y) - I_{DF}(x, y)}{I_{BF}(x, y)}\right). \quad (1)$$

A representative bright-field normalized image is shown in Figure 1.

C. GPU-accelerated particle tracking

The goal of a particle tracking algorithm is to output the three-dimensional position of a particle center as a function of time, given a sequence of video frames as input. Existing algorithms can find the position of spherical particles to sub-pixel in-plane accuracy and similar out-of-plane accuracy.[8,21,22] Despite their accuracy, existing tracking routines throttle data throughput due to their serial nature. To increase throughput, we implemented a GPU algorithm using CUDA architecture[23] to massively parallelize the task of obtaining three-dimensional particle positions.

We measured bead positions from images using a centroid-finding algorithm frequently used in magnetic-

tweezer instruments.[8,18] The in-plane (X-Y) position of the bead is found by measuring the linear intensity profile along the horizontal and vertical axis of the bead near the center. A cross-correlation of the linear intensity profile with its mirror image is used to find a first guess for the in-plane particle center. The cross-correlation is fit to a second-degree polynomial near the central point to find the in-plane particle center to sub-pixel accuracy.

Once we have calculated the X-Y position, we can find the out-of-plane (Z) position. First, a radial intensity profile about the X-Y center is compared to a previously generated radial-intensity vs height look-up table. The look-up table is generated using the same in-plane tracking algorithm, but with bead height varied in 100 nm steps by a piezoelectric stage. Second, the look-up-table is interpolated using least squares with polynomial fitting to find the height of the particle.

To capture a high-speed event, we first preview data at approximately 50 frames per second while the camera continuously updates the latest 16 GB of video on an internal circular buffer of memory. When we observe an event of interest in the preview data, we trigger the camera to dump the buffer, and the data processing begins. The camera sends packets, each containing multiple camera frames, each containing multiple bead images, from the hs-CMOS to the CPU (see Figure 2). The CPU relays the packets via the PCI-express bus to the graphics processing unit (GPU), where particle positions are determined for all of the beads in the packet. With our tracking algorithm, we have tracked thousands of beads simultaneously and have obtained particle position data at the limit of the ethernet cable image transfer rate. Our GPU-accelerated particle-tracking algorithm is freely available for download at http://www.engr.ucsb.edu/~saleh/#Code and can be used by anyone with an NVidia CUDA 2.0 capable GPU. Our code can be extended to include rotational tracking, bright field normalization, and even alternate methods of particle tracking.

D. Flowcell preparation

We prepared glass coverslips by rinsing with acetone, isopropyl alcohol (IPA), de-ionized water, drying with nitrogen gas, then plasma treating for 10 min. A solution of 2.5 μm diameter polystyrene beads suspended in IPA was evaporated onto the bottom coverslip surface to leave randomly dispersed beads that subsequently became the "stuck bead" fiducial markers to track coverslip drift (Figure 3). Once the IPA evaporated, coverslips were left on a hotplate for 3 min at 145 °C. Sigmacote solution was pipetted onto the coverslip and allowed to air-dry in a fume hood. Residual Sigmacote clumps were removed with an ethanol rinse. The flowcell was assembled by sandwiching a piece of parafilm, cut using a 40 W CO_2 laser (Full Spectrum), between the bottom and top coverslips. The flowcell was placed on a hotplate at 80 °C for 10 min to seal the parafilm to the glass.

The double-stranded DNA (dsDNA) used for thermal noise analysis was taken from pGluc-basic 2 vector (NEB).

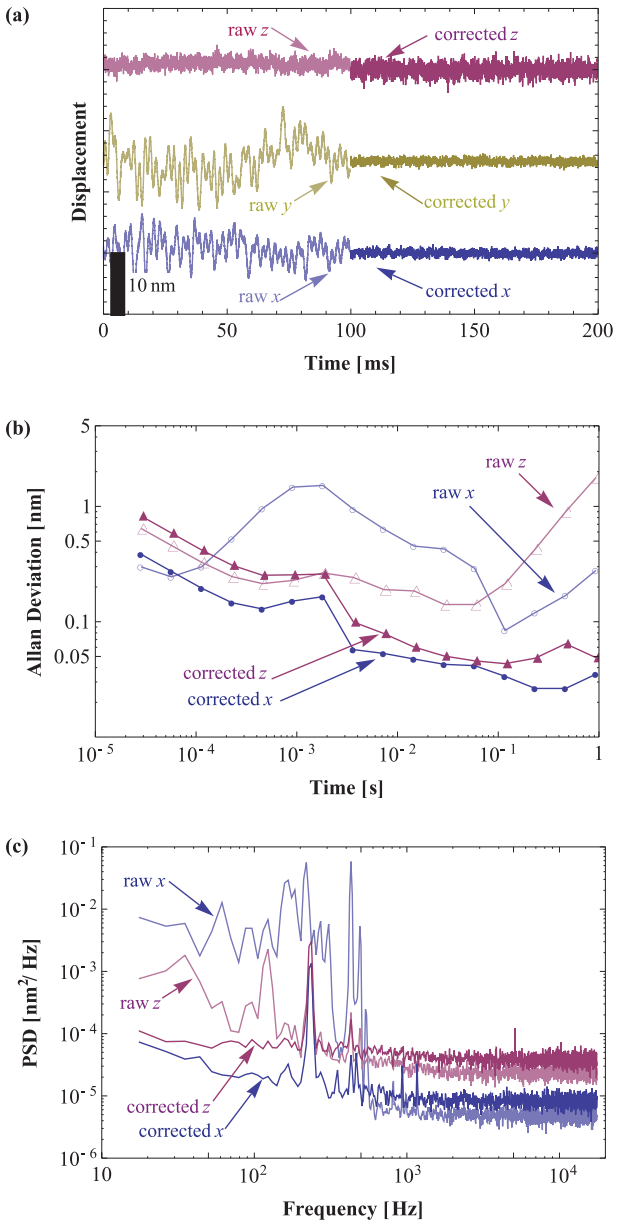

FIG. 3. Three ways to examine the instrumental tracking error of a magnetic tweezer. Figure 3(a) shows the position of a partially molten polystyrene reference bead as a function of time with (corrected) and without (raw) reference bead subtraction. Figure 3(b) shows the Allan deviation of bead position as a function of the measurement time, for lateral X and axial Z fluctuations. Figure 3(c) shows the PSD of bead motion, with and without reference bead subtraction. For clarity, lateral Y-fluctuation data is not shown in Figures 3(b) and 3(c), but it qualitatively matches the X-fluctuation data.

The vector was digested by AvaI to yield fragments of 3392-bp and 1566-bp length (data in Figure 4). Our dsDNA molecules have two moieties for tethering: a biotin label, and a digoxigenin label bound to an anti-digoxigenin (anti-dig) anitbody. The dsDNA was left in a fridge for 40 min to allow the anti-dig to non-specifically bind to the Sigmacote surface, leaving sparse surface-anchored dsDNA. Biotin-streptavadin bonds were formed by flowing streptavadin-coated 1.05 μm diameter magnetic beads in TE buffer into the flowcell, and allowing the beads to diffuse around the coverslip surface and find dsDNA molecules for 10 min.

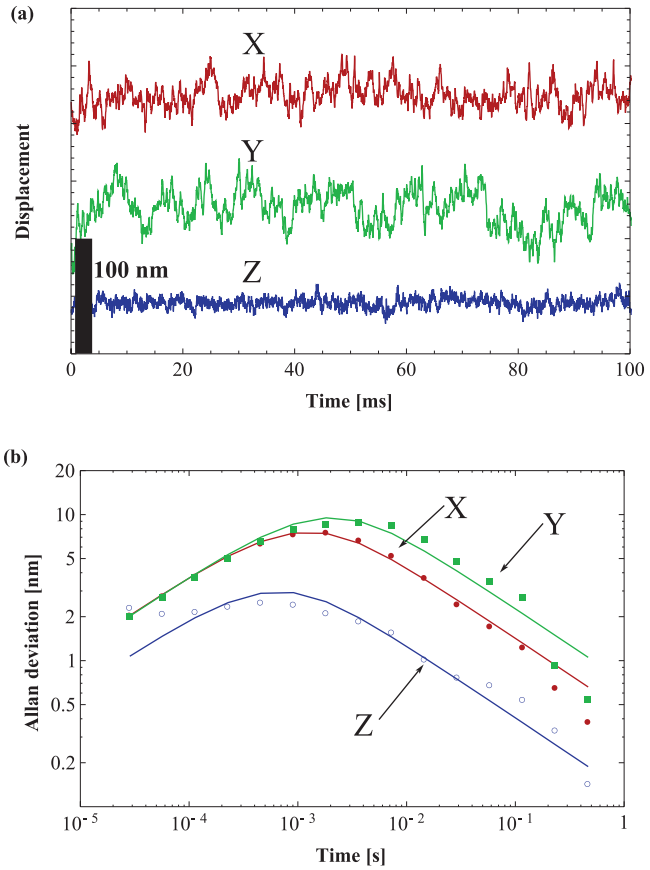

FIG. 4. The time-domain X,Y,Z positions of a magnetic bead tethered to a 1566 bp dsDNA molecule (Figure 4(a)) can be analyzed using Allan deviation (Figure 4(b)). Best-fit curves to Allan deviation data give measurements of the trap stiffness κ and probe drag α.

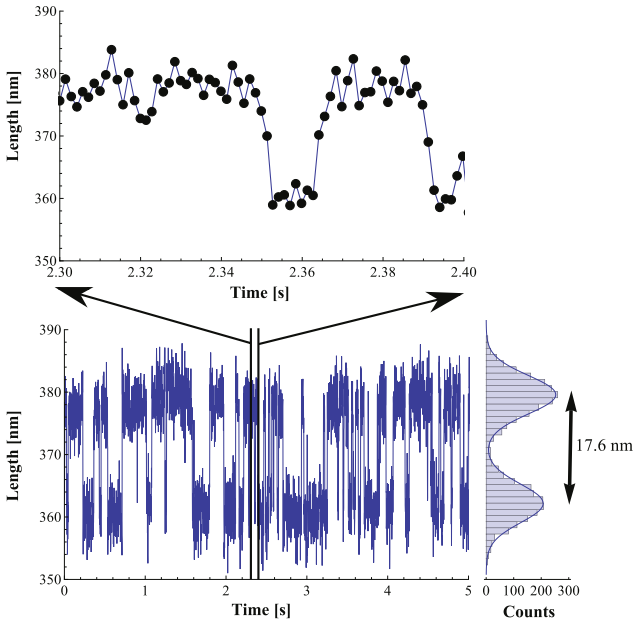

FIG. 5. Extension trajectory of a DNA hairpin undergoing stochastic folding/unfolding transitions. Data was acquired at 35087 fps, then low-pass filtered to 701.74 fps. Inset shows a 0.011 s residence in the folded state. The histogram of particle positions is well-described by a sum of two Gaussians, separated by 17.6 nm.

DNA hairpin measurements in Figure 5 were performed on a DNA hairpin structure described previously,[24] consisting of a 20-bp stem sequence with 55% GC content and a thymidine tetraloop. dsDNA handles were attached via non-palindromic ligation sequences at either end of a PAGE-purified DNA oligomer (Integrated DNA Technologies). Abasic sites were also included to provide space between the hairpin stem and handles. For the 5′ handle, we generated 1050-bp DNA with a terminal digoxigenin and 15-nt overhang sequence by autosticky PCR.[25] We prepared the 3′ handle by annealing a 20-nt oligo with a terminal biotin.

III. EXPERIMENTAL MEASUREMENTS

A. Stuck beads

To determine the instrumental noise of our system, we measured the position vs time of polystyrene particles stuck to a glass coverslip surface. In Figure 3(a) we plot the position versus time of a single particle (raw) and that same particle with the position of a second stuck reference bead subtracted (corrected) in order to compensate for common-mode noise. In Figure 3(b) we plot the Allan deviation, the square root of the Allan variance, which characterizes the noise at various timescales.[26,27] In principle, the Allan deviation contains the same information as the power spectral density (PSD) graph shown in Figure 3(c), but we find that the Allan deviation more clearly illustrates the relevant noise regimes. At very short time scales, below 10^{-4} s, the noise is dominated by the limited accuracy of our particle tracking algorithm. At intermediate times, we see the introduction of common-mode acoustic noise in the raw traces. We note that the common-mode noise is reduced by three orders of magnitude in the lateral direction after reference correction. At times above 0.1 s, we see the influence of thermal drift in both the lateral and axial traces. With reference bead correction, the axial noise reaches 0.6 Å at down-sampling times beyond 1/60 s, which compares favorably to previous measurements that attained 5 Å in similar conditions.[8]

B. DNA tether

The tethered probe particles in magnetic tweezers are micron-sized superparamagnetic beads that fluctuate due to thermal collisions with surrounding water molecules. To a good approximation, the particles can be modeled as massless Brownian particles with drag coefficient α trapped within the constraints of a harmonic potential of stiffness κ. In Figure 4(b), we fit the analytical equation for the Allan deviation for a tethered Brownian particle[27,28] to experimental data using a 1566-bp dsDNA molecule in the X and Y directions, resulting in $\alpha_x = 1.78 \times 10^{-8}$ N s/m, $\alpha_y = 1.86 \times 10^{-8}$ N s/m, $\kappa_x = 2.87 \times 10^{-5}$ N/m, and $\kappa_y = 1.61 \times 10^{-5}$ N/m.

We are therefore able to resolve a corner frequency of $f_{c,x} = \frac{\kappa_x}{2\pi\alpha_x} = 256$ Hz, beyond the Nyquist frequency of conventional magnetic tweezers. The Allan variance in the axial Z-direction has added instrumental noise at timescales below 1 ms that makes a direct fit to analytical theory impossible.

However, we can measure the length with 1 nm of noise at 100 Hz.

C. DNA hairpin dynamics

To demonstrate the ability of the high-speed magnetic tweezer to accurately measure a fast biomolecular transition, we measured a DNA hairpin as it fluctuated between a folded and an unfolded state (see Figure 5). The upper inset shows a transient closed hairpin state that was only stable for 8 frames at 701.74 fps, or 0.011 s, faster than a single frame of the traditional 60 Hz CCD camera. The right inset is a histogram of particle positions, with a best-fit curve that is a sum of two Gaussian peaks with a separation of 17.6 nm, in reasonable agreement with previous results of 18.1 ± 0.3 nm.[24]

IV. CONCLUSION

We have developed a high-speed magnetic tweezer that utilizes a SLD for illumination and a hs-CMOS camera for detection. To handle the increased data throughput of the high-speed camera, we have re-written a particle-tracking algorithm to utilize a GPU for faster data throughput. Our particle tracking results on a dsDNA tether have demonstrated our ability to resolve corner frequencies above 250 Hz. We have accurately resolved DNA hairpin dynamics that were unresolvable with previous generations of magnetic tweezers. We have shown how the high-speed magnetic tweezer has noise below 0.6 Å in three dimensions at a bandwidth of 100 Hz. We expect that this instrument will be applied to problems requiring high-speed resolution of biomolecular events, including fast folding/unfolding processes, and stepping motions of motor proteins.

ACKNOWLEDGMENTS

We thank S. Pennathur and T. Wynne for use of their hs-CMOS cameras during the early stages of this project. We thank C-Y Park for providing dsDNA tethers and for useful discussions. We thank O. Bertrand, D. McIntosh, N. Ribeck, J. Berezney, and F. Henderikx Freitas for helpful discussions. B.L. acknowledges support from a NSERC PGS-D fellowship. S.T. thanks UCSB-RISE. We acknowledge support from NSF Grant No. PHY-0748564.

[1] W. J. Greenleaf, M. T. Woodside, and S. M. Block, Annu. Rev. Biophys. Biomol. Struct. **36**, 171 (2007).
[2] K. C. Neuman and A. Nagy, Nat. Methods **5**, 491 (2008).
[3] Y. R. Chemla, Phys. Chem. Chem. Phys. **12**, 3080 (2010).
[4] E. A. Abbondanzieri, W. J. Greenleaf, J. W. Shaevitz, R. Landick, and S. M. Block, Nature (London) **438**, 460 (2005).
[5] A. R. Carter, Y. Seol, and T. T. Perkins, Biophys. J. **96**, 2926 (2009).
[6] M. Mahamdeh, E. Schäffer, *et al.*, Opt. Express **17**, 17190 (2009).
[7] W. Cheng, S. G. Arunajadai, J. R. Moffitt, I. Tinoco, Jr, and C. Bustamante, Science **333**, 1746 (2011).
[8] N. Ribeck and O. A. Saleh, Rev. Sci. Instrum. **79**, 094301 (2008).
[9] N. Ribeck, D. L. Kaplan, I. Bruck, and O. A. Saleh, Biophys. J. **99**, 2170 (2010).
[10] W. J. Greenleaf, M. T. Woodside, E. A. Abbondanzieri, and S. M. Block, Phys. Rev. Lett. **95**, 208102 (2005).
[11] J. R. Moffitt, Y. R. Chemla, S. B. Smith, and C. Bustamante, Annu. Rev. Biochem. **77**, 205 (2008).
[12] I. De Vlaminck and C. Dekker, Ann. Rev. Biophys. **41**, 453 (2012).
[13] K. Kim and O. A. Saleh, Nucleic Acids Res. **37**, e136 (2009).
[14] W. P. Wong and K. Halvorsen, Opt. Lett. **34**, 277 (2009).
[15] O. Otto, J. L. Gornall, G. Stober, F. Czerwinski, R. Seidel, and U. F. Keyser, J. Opt. **13**, 044011 (2011).
[16] O. Otto, F. Czerwinski, J. L. Gornall, G. Stober, L. B. Oddershede, R. Seidel, and U. F. Keyser, Opt. Express **18**, 22722 (2010).
[17] G. M. Gibson, R. W. Bowman, A. Linnenberger, M. Dienerowitz, D. B. Phillips, D. M. Carberry, M. J. Miles, and M. J. Padgett, Rev. Sci. Instrum. **83**, 113107 (2012).
[18] C. Gosse and V. Croquette, Biophys. J. **82**, 3314 (2002).
[19] J. Lin and M. T. Valentine, Rev. Sci. Instrum. **83**, 053905 (2012).
[20] S. H. Lee, Y. Roichman, G. R. Yi, S. H. Kim, S. M. Yang, A. Van Blaaderen, P. Van Oostrum, and D. G. Grier, Opt. Express **15**, 18275 (2007).
[21] J. Lipfert, J. W. Kerssemakers, M. Rojer, and N. H. Dekker, Rev. Sci. Instrum. **82**, 103707 (2011).
[22] M. T. J. van Loenhout, J. W. J. Kerssemakers, I. De Vlaminck, and C. Dekker, Biophys. J. **102**, 2362 (2012).
[23] J. Sanders and E. Kandrot, *CUDA by Example: An Introduction to General-Purpose GPU Programming* (Addison-Wesley Professional, 2010).
[24] M. T. Woodside, W. M. Behnke-Parks, K. Larizadeh, K. Travers, D. Herschlag, and S. M. Block, Proc. Natl. Acad. Sci. U.S.A. **103**, 6190 (2006).
[25] J. Gal, R. Schnell, S. Szekeres, and M. Kalman, Mol. Gen. Genet. **260**, 569 (1999).
[26] F. Czerwinski, A. C. Richardson, and L. B. Oddershede, Opt. Express **17**, 13255 (2009).
[27] B. M. Lansdorp and O. A. Saleh, Rev. Sci. Instrum. **83**, 025115 (2012).
[28] A. J. W. Te Velthuis, J. W. J. Kerssemakers, J. Lipfert, and N. H. Dekker, Biophys. J. **99**, 1292 (2010).